Microchim Acta (2017) 184:2949–2957
DOI 10.1007/s00604-017-2267-3

ORIGINAL PAPER

A gold electrode modified with a three-dimensional graphene-DNA composite for sensitive voltammetric determination of dopamine

Liping Lu[1] · **Linqing Guo**[1] · **Tianfang Kang**[1] · **Shuiyuan Cheng**[1]

Received: 23 September 2016 / Accepted: 13 April 2017 / Published online: 12 May 2017

Abstract The authors describe a three-dimensional (3D) structure composed of graphene and DNA for use in a voltammetric dopamine (DA) sensor. The material was deposited on a gold electrode, and the enhanced charge-transfer performance and deposition of DNA were confirmed by electrochemical analysis. Atomic force microscopy shows the graphene-DNA composite to have been assembled on the modified gold electrode. The modified gold electrode possesses excellent electrocatalytic activity for determination of DA, best at a working voltage of 0.1 V (vs. SCE). Ascorbic acid does not interfere. Response to DA is linear in the 0.1 to 100 μM concentration range, with a 30 nM detection limit even in the presence of 1.0 mM of ascorbic acid.

Keywords AFM · Electrochemical impedance spectroscopy · DNA · Hexacyanoferrate · Laviron theory

Introduction

Dopamine (DA) plays a significant role in the function of the central-nervous, renal, and hormonal systems as an important neurotransmitter. DA is believed to be related to several diseases, and low levels of DA may cause neurological disorders, such as Parkinson's disease, schizophrenia, and Huntington's disease [1]. Precise and efficient detection of DA is needed in order to gain a better understanding of its physiological functions and mechanisms of action in the human body. However, the basal concentration of DA is low (10–1000 nM), and ascorbic acid (AA), which has similar properties, is an interfering compound. There are many methods for the detection of DA, such as high-performance liquid chromatography-mass spectrometry, fluorescence spectrometry, and electrochemical and electrochemiluminescence techniques. Among these methods, electrochemical sensors are the most promising and desirable for diagnostic sensing owing to their rapid response, high sensitivity, ease of operation, and low cost [2]. However, electrochemical detection of DA is always subject to interference by ascorbic acid (AA), which coexists with DA in biological samples and has a similar oxidation potential. The complete elimination of AA interference thus merits further investigation.

Graphene has attracted much attention because of its unique physical and chemical properties [3]. As a nanosheet, its excellent electronic transport properties, high mechanical strength, and high surface area have stimulated considerable research in graphene-based applications, such as sensors, nanoelectronics, and supercapacitors [4]. Duplex DNA-stored genetic information has a unique and perfect structure, with aromatic heterocycles of base pairs extending in parallel along a helical axis. Its well-stacked base pairs have charge transfer properties [5], but can also be used as a recognition element in electrochemical sensors.

Effective Assembly is a powerful technique for the construction of hierarchical graphene-based architectures with novel functionalities [6]. In particular, the assembly of nanoscale graphene into three-dimensional (3D) hierarchical architectures

Electronic supplementary material The online version of this article (doi:10.1007/s00604-017-2267-3) contains supplementary material, which is available to authorized users.

✉ Liping Lu
lipinglu@bjut.edu.cn

[1] Key Laboratory of Beijing on Regional Air Pollution Control, Beijing University of Technology, Beijing 100124, China

produces new physiochemical properties which are remarkably different from those of both the individual building blocks and the bulk materials, extending the possible applications of graphene [7]. Over the past five years, graphene-DNA hybrid materials have attracted much attention because of their great promise in the fields of hydrogels [8], drug delivery [9], aptamer sensors [10], sensor arrays [11], nanocomposites [12], and surface plasmon resonance chips [13]. However, little attention has been paid to the charge-transfer capability of graphene-DNA hybrid materials. We are interested in the rapid charge transfer capabilities of stacked base pairs in double-stranded DNA and the electronic transport properties of graphene [14], due to their potential for application in electronics, photonics, sensors, and chip fabrication [15].

Many graphene-based materials have been used to fabricate the electrochemical interface for sensing DA [16–19]. However, these compounds are mostly immobilized on a glassy carbon electrode, which limits the application of these sensors, such as in chips for clinical tests. In this article, we report on controllable and ordered of graphene quantum dots (GQDs) and DNA, as shown in Scheme 1. Here, a gold electrode was used as the base interface for the construction of an electrochemical sensor. A superimposed 3D structure of graphene-DNA was fabricated based on layer-by-layer (LbL) assembly.

Experimental

Materials and reagents

1-(3-Dimethylaminopropyl)-3-ethylcarbodiimide hydrochloride (EDC), 6-mercapto-1-hexanol (MCH), hexammineruthenium(III)-Ru(NH_3)$_3$$Cl_3$ (RuHex), DA hydrochloride, and acidum ascorbicum (AA) were purchased from Sigma Chemical Co. Ltd. (www.sigmaaldrich.com). *N*-hydroxysuccinimide (NHS) was purchased from Sinopharm Chemical Reagent Co, Ltd. (en.reagent.com.cn) graphene oxide (GO) and graphene quantum dots were purchased from Nanjing XFNANO Materials Tech Co., Ltd. (http://m.xfnano.com, China). NaCl, NaH_2PO_4, Na_2HPO_4, $K_3[Fe(CN)_6]$, $K_4[Fe(CN)_6]$, and KCl were purchased from Beijing Chemical Works (www.beijingchemworks.com, China). All reagents were of analytical grade. Ultrapure water prepared using a Milli-Q system (Millipore, www.merck-china.com) was used in all of the experiments. The four labeled single-stranded oligonucleotides (ss-DNA) used in the experiments were synthesized by Shanghai Sangon Biotechnology Corporation (www.sangon.com, China). The sequences of the four ss-DNA used in this work are given in Table 1.

All of the double-stranded DNA (dsDNA) were obtained by the hybridization of ssDNA using a Bio-RAD T100 thermal cycler in phosphate buffer (5 mM 0.1 M NaCl, pH = 7.4). $dsDNA_1$ was obtained by mixing ssDNA-1 and ssDNA-2 in a 1:1 M ratio and then incubating at 90 °C for 1 min before slowly cooling to room temperature. $dsDNA_1$ was assembled on the gold electrode surface. $dsDNA_2$ was formed by hybridization of ssDNA-3 and ssDNA-4 using the same process as described above and then assembled on the GQD surface.

Apparatus and measurements

Electrochemical measurements were performed on a CHI660E electrochemical workstation with a conventional

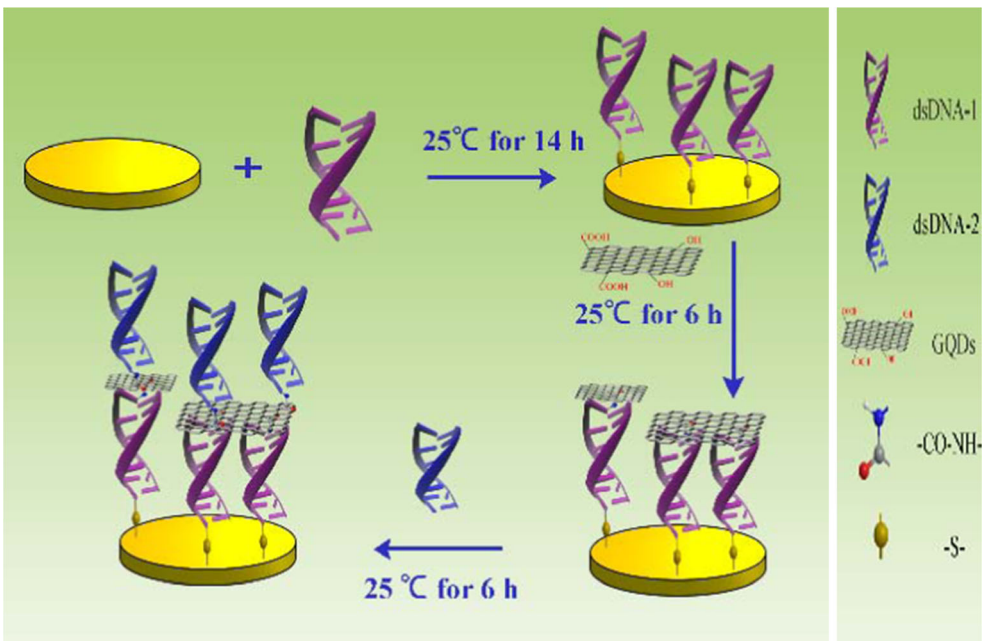

Scheme 1 Schematic diagram of the GQDs with DNA and the subsequent fabrication of multi-layered GQD-DNA electrodes

Table 1 Sequences of the four ss-DNA used in this Work

	Sequence
ssDNA-1	5′-NH_2-C6-CGT CCG A-3′
ssDNA-2	5′-SH-C6-TCG GAC G-3′
ssDNA-3	5′-CGT CCG A-3′
ssDNA-4	5′-NH_2-C6-TCG GAC G-3′

three-electrode cell (Shanghai CH Instrument Company, China). A modified gold electrode was used as the working electrode. A saturated calomel electrode (SCE) and a platinum wire were used as the reference and counter electrodes, respectively. The surface morphologies of the modified gold electrode were determined using a Dimension 3100 atomic force microscope (Bruker, USA).

Fabrication of the sensor

Before sensor fabrication, the gold electrodes (diameter = 2 mm) were polished with alumina slurries (0.02 ~ 0.05 μm) on soft microfiber polishing pads. The gold electrodes were then purified by treatment with a piranha solution consisting of 70% concentrated sulfuric acid and 30% hydrogen peroxide for 20 min. Next, sonication was performed, followed by successive ultrasonic cleaning for 3 min in ultrapure water, then ethanol, then ultrapure water. The electrode was allowed to dry in N_2. $dsDNA_1$ (10 μL of 50 μM) was assembled on the clean gold electrode via S-Au at room temperature for 14–18 h in a humid environment with 100 mM $MgCl_2$ to form the monolayer $dsDNA_1$. The electrode was then backfilled with 6-mercapto-1-hexanol in phosphate buffer for 60 min. Following this, GQDs (1 mg mL^{-1}, 10 μL) with 0.1 M EDC (1 μL) and 0.1 M NHS (0.5 μL) were coated onto the $dsDNA_1$ modified gold electrode for 6 h at room temperature in a humid environment. The modified electrode was named the GQD/$dsDNA_1$/Au. Finally, $dsDNA_2$ solution (10 μL of 50 μM) with 0.1 M EDC (1 μL) and 0.1 M NHS (0.5 μL) was dropped onto the GQD/$dsDNA_1$/Au electrode for 6 h under the same conditions. After each step in the assembly process, the electrode surface was rinsed thoroughly with phosphate buffer and ultrapure water to remove nonspecifically absorbed materials and then dried with nitrogen stream.

Electrochemical measurements of the sensor

To detect dopamine, the $dsDNA_2$/GQD/$dsDNA_1$/Au electrode was incubated in dopamine solution for 15 min (the optimal conditions), and the measurement of dopamine was then conducted on a CHI660a electrochemical workstation with a potential range of −0.2 ~ 0.4 V. Differential pulse voltammetry (DPV) was used for selective detection of DA throughout.

Results and discussion

Choice of materials

Among graphene and its derivatives, graphene quantum dots are characterized by a well-defined structure, consisting of a few layers of nanosheet, and have edge effects and oxygen-containing groups (Fig. S1). Moreover, their large surface area, water solubility and low cytotoxicity make them more suitable for sensor applications. [20] The rapid charge transfer of stacked base pairs in double-strand DNA and the electronic transport properties of GQDs have been noted. In addition, DNA can be a good probe for the sensitive detection of neurotransmitters [21, 22]. It is concluded that using DNA and graphene as the sensing element may result in the sensitive detection of DA.

Morphological characterization of the modified electrode

Atomic force microscopy (AFM) was used to directly visualize the morphology of a freshly gold sprayed mica surface following the immobilization of the DNA and GQDs. Figure 1 shows a sequence of AFM images showing the modification process of the gold surface. The 2D images of $dsDNA_1$/Au, GQD/$dsDNA_1$/Au, and $dsDNA_2$/GQD/$dsDNA_1$/Au show that they all have uniform morphologies and that each morphology is different. The typical top view of dsDNA assembled on the gold surface in Fig. 1a shows spherical particles [23]. When GQD sheets cover the top of $dsDNA_1$, the surface becomes smoother (Fig. 1b). These spherical particles join into ribbons, which is consistent with the scheme. $dsDNA_2$ was then immobilized on the GQD surface, and particles formed, again. Therefore, each assembly process is in accordance with Scheme 1. In addition, X-ray photoelectron spectroscopy (XPS) of the high-resolution C1s peaks confirmed that C = C, C = O bands exist on the sensor interface (Fig. S2). Moreover, the changes of the area of C1s spectra of dsDNA1/Au, GQD/$dsDNA_1$/Au, $dsDNA_2$/GQD/$dsDNA_1$/Au are reasonable. These results show that bio-nano-structures were formed.

The heights of the particles were obtained from 3D images and their height profiles. The uniformity in height shows that GQDs and DNA are free of superposition and do not overlap. As shown in Fig. 1b′ and c′, the average height of dsDNA and the GQDs is about 2 nm. This is similar to the length of the 7 base pair dsDNA (the length of 3 bases is about 1 nm) and the thickness of the GQD. The height analysis extracted from typical AFM images confirmed that DNA-GQD assembly resulted in a layered bio-nanostructure. The bonding groups on graphene and DNA efficiently guide the assembly process, which facilitates the controllable assembly of graphene and DNA into precise and predictable architectures.

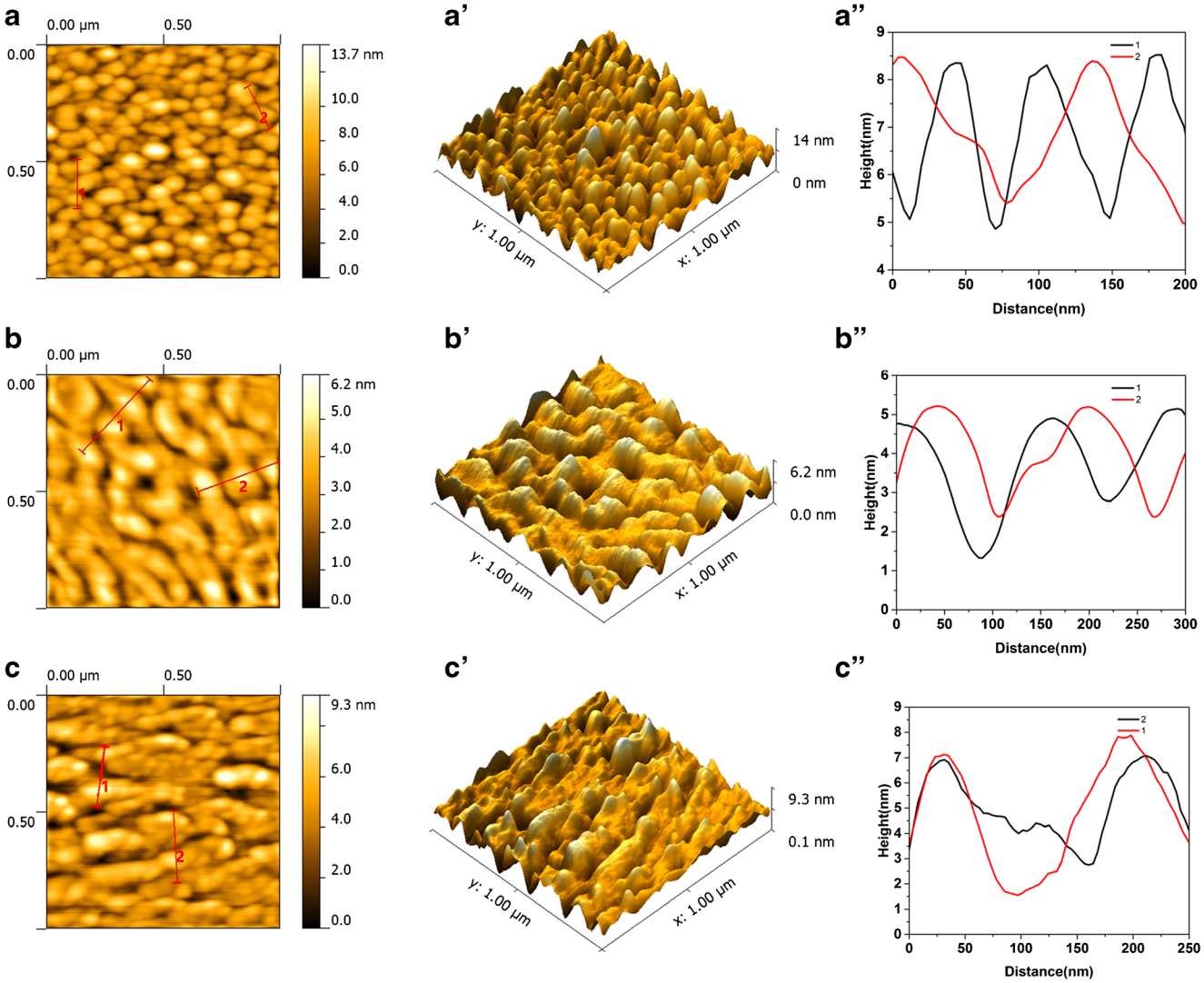

Fig. 1 AFM image: $dsDNA_1$ on the gold interface (2D image (**a**), 3D image (**a'**) and height profile (**a''**)); GQDs on the $dsDNA_1$/Au (2D image (**b**), 3D image (**b'**) and height profile (**b''**)); $dsDNA_2$ on the GQD/$dsDNA_1$/Au (2D image(**c**), 3D image (**c'**) and height profile (**c''**))

Electrochemical impedance spectroscopy analysis

Electrochemical impedance spectroscopy (EIS) is a highly effective method for probing the features of a surface-modified electrode using a $[Fe(CN)_6]^{-3/-4}$ redox probe. In this study, EIS was performed in order to investigate changes in the charge-transfer resistance (Rct) of each surface modification step, as shown in Fig. 2. For the bare gold electrode, the impedance spectrum includes a semicircular portion at higher frequencies, which is related to the electron-transfer-limited process and a linear part at lower frequencies corresponding to diffusion. The increase in the diameter of the semicircle reflects the increase in the interfacial charge-transfer resistance. As shown Fig. 2, in the case of the bare gold electrode immobilized $dsDNA_1$, the value of Rct increased to 2000 Ω. This is because the immobilization of negatively charged $dsDNA_1$ on the electrode surface results in a negatively charged interface which electrostatically repels the negatively charged $[Fe(CN)_6]^{-3/-4}$ redox probe and inhibits interfacial

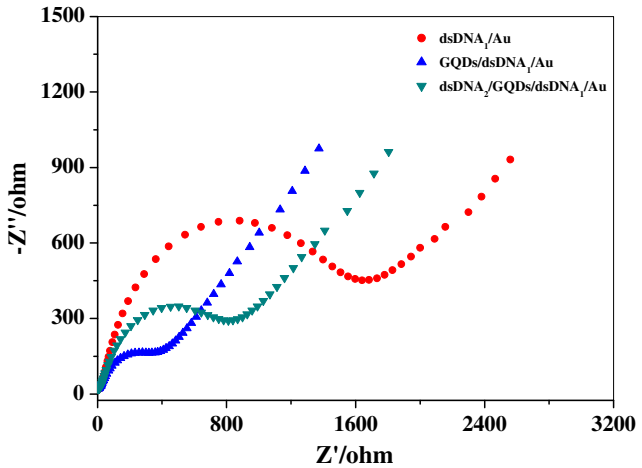

Fig. 2 Electrochemical impedance spectroscopy of electrode with 5 mM $K_3[Fe(CN)_6]$/ $K_4[Fe(CN)_6]$

charge transfer [24]. Subsequently, GQDs were fixed on the top of the $dsDNA_1$, and the value of R_{ct} decreases from 2000 to 600 Ω. GQD-modified $dsDNA_1$/Au (GQD/$dsDNA_1$/Au) showed a much smaller Rct value than $dsDNA_1$/Au, indicating that GQDs are an excellent electrically conducting material for the acceleration of electron transfer [25]. After $dsDNA_2$ was loaded onto the GQD/$dsDNA_1$/Au, the value of Rct greatly increased to 1000 Ω, which is higher than that for GQD/$dsDNA_1$/Au under the same conditions. This result is attributed to the large amount of $dsDNA_2$ linked to GQDs.

Cyclic voltammetry (CV) is also an effective method for probing the features of a surface-modified electrode, as shown in Fig. S3. The CV curves show that GQDs greatly promote electron transfer and the relative magnitude of the redox peak currents is as follows: GQD/$dsDNA_1$/Au > $dsDNA_2$/GQD/$dsDNA_1$/Au > $dsDNA_1$/Au. These results are consistent with EIS. Considering the results of EIS and CV, the electrode appears to have been formed by layer-by-layer superimposition, producing a 3D structure.

Electron transfer analysis

In order to improve sensor sensitivity, different methods have been used, such as catalysis, circulation amplification and increased electrode area. Of course, a higher intensity electron transfer interface will result in highly sensitive detection. Laviron theory was used to determine the electron-transfer rate constant (k_s) of this sensor depending on RuHex redox [26, 27]. Fig. S4 (a'), (b'), and (c') show plots of the peak potential (E_{pc}) versus the natural logarithm of the scan rate (ln υ). In the scan rate range 1–13 V/s, the plots of E_{pc}-$E^{o\prime}$ against ln υ are linear with slopes of -RT/αnF for the cathodic peak [28]. k_s can be obtained by means of the Laviron equation (Table 2). An increasing DNA-mediated charge-transfer rate is observed in this system, which is 7.26 s^{-1} when the GQDs link to $dsDNA_1$ and $dsDNA_2$ compared with 5.94 s^{-1} for $dsDNA_1$/Au. However, charge transfer in DNA is more difficult when GO is linked to $dsDNA_2$ and $dsDNA_1$ (electron-transfer rate 5.26 s^{-1}). The experimental results clearly indicate faster electron transfer at the $dsDNA_2$/GQD/$dsDNA_1$/Au interface. As a carbon-based nanomaterial, GQDs have a highly efficient electron-transfer rate, which promotes electron transfer between the DNA probe and the electrode surface. Similar behavior was observed on the modified electrodes in the presence of the $[Fe(CN)_6]^{-3/-4}$ couple by EIS (Fig. 2), confirming the CV results.

Table 2 Surface Coverage, Γ, and the ET Rate Constant, Ks, Estimated for $dsDNA_1$/Au, $dsDNA_2$/GQD/$dsDNA_1$/Au and $dsDNA_2$/GO/$dsDNA_1$/Au

	Ks /s (CV)	Γ pmol cm^{-2}
$dsDNA_1$/Au	5.94	8.83
$dsDNA_2$/GQD/$dsDNA_1$/Au	7.26	11.47
$dsDNA_2$/GO/$dsDNA_1$/Au	5.26	1.23

Quantification of immobilized DNA

The amount of the DNA on the electrode surface can be estimated using the effective surface concentration:

$$\Gamma_{DNA} = \frac{Q}{nFA}\frac{Z}{m} \quad (1)$$

where A is the electrode area in cm^2 (0.03 cm^2), z is the charge on RuHex (z = 3), m is the number of bases in the duplex DNA (m = 7), and Q is the reductive signal from RuHex minus the redox reporter signal from the phosphate buffer. Using eq. 1, the Γ values were calculated to be 8.83 and 11.47 pmol cm^{-2} for $dsDNA_1$/Au and $dsDNA_2$/GQD/$dsDNA_1$/Au respectively (Table 2), indicating a clear increase in the amount of DNA on the surface of the GQDs compared to gold. This behavior can be attributed to the high surface area of GQDs providing ultrahigh loading capacity for analytical molecules [29]. In addition, graphene oxide (GO) was used in place of GQDs to fabricate $dsDNA_2$/GO/$dsDNA_1$/Au, and the Γ value of $dsDNA_2$ was 1.23 pmol cm^{-2}. This can be attributed to differences between the structures of GQDs and GO. There are more COO^- groups on the GQDs than on the GO surface per unit area. These connect with amino-modified DNA ($dsDNA_2$). Therefore, GQDs a have higher immobilization capacity than GO does.

Electrochemical behavior of dopamine on the sensors

Figure 3 shows differential voltammetry of 200 μM DA in 0.1 M phosphate buffer at the bare gold and modified electrodes. The differential voltammetry (DPV) curve of bare gold shows a slight peak current at 0.1 V (Fig. 3, curve a), which is in agreement with the electrochemical behavior of DA in

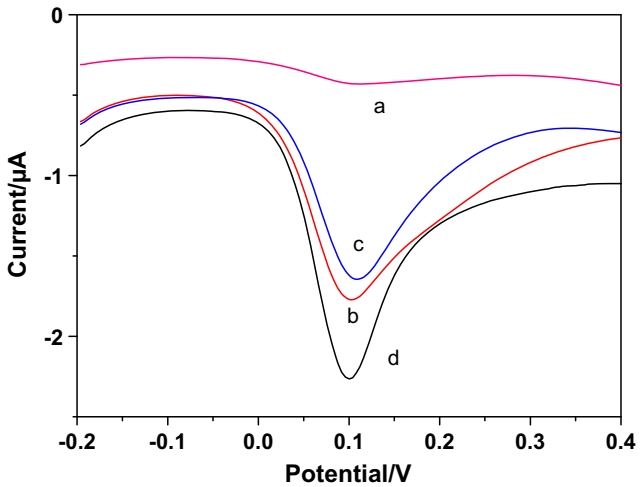

Fig. 3 Differential Pulse Voltammetry curves in 0.1 M phosphate buffer (pH 7.4) containing 200 μM DA, at bare Au (a), $dsDNA_1$/Au(b), GQD/$dsDNA_1$/Au(c) and $dsDNA_2$/GQD/$dsDNA_1$/Au(d)

previous reports [1, 30, 31]. The peak current clearly increases after $dsDNA_1$ assembly on the gold surface (Fig. 3, curve b). This is because at the measured acidity (pH 7.4), DA (pK_a = 8.9) is positively charged. Therefore, protonated DA easily permeates into and accumulates within negatively charged $dsDNA_1$ on the electrode interface by electrostatic attraction, which results in a large redox response [21].

Curve c in Fig. 3 shows a better electrochemical response for DA sensing at GQD/$dsDNA_1$/Au than at the bare Au electrode. This indicates that the π-interaction between the aromatic ring of DA and graphene may accelerate electron transfer, which increased the DA response. However, the peak current of DA is slightly less than that for $dsDNA_1$/Au. Therefore, it is concluded that DNA modification is better for the DA electrochemical response. After $dsDNA_2$ was immobilized on the GQDs, the peak current of DA was higher than with the other electrodes. This is not only due to the DNA effect, but also reasoned by the increased amount of DNA on the GQD surface.

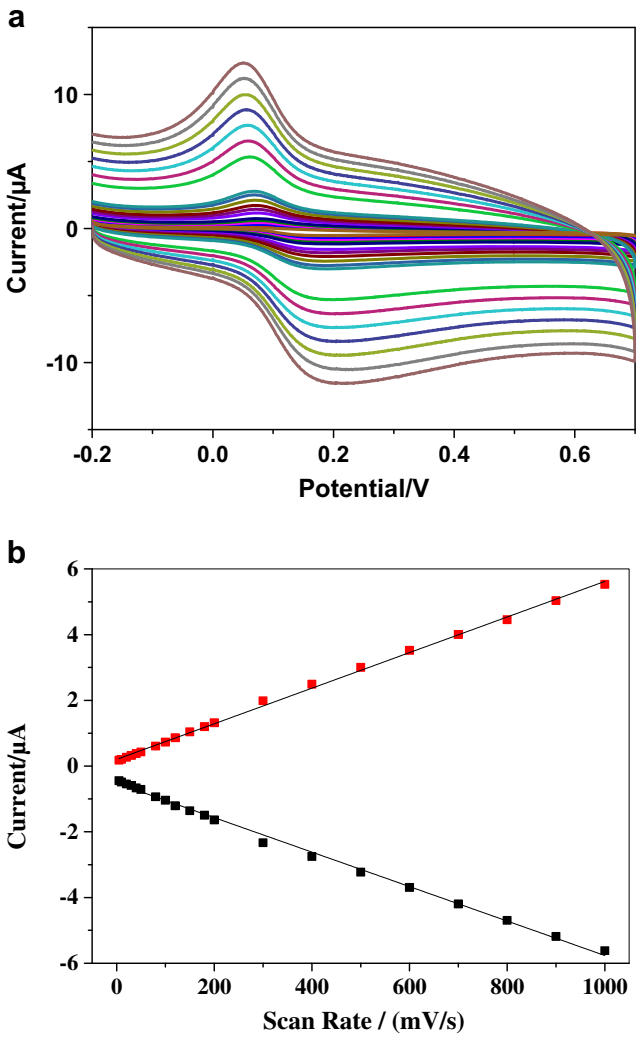

Fig. 4 **a** Effect of scan rate on the cyclic voltammograms of DA with $dsDNA_2$/GQD/$dsDNA_1$/Au in 0.1 M phosphate buffer (pH 7.4) at 5, 10, 20, 30, 40, 50, 80, 100, 120, 150, 180, 200, 300, 400, 500, 600, 700, 800, 900, 1000 mV s^{-1}. **b** Plots of peak currents (i) vs. scan rate

Effect of the scan rate

To further investigate the electrochemical behavior of DA at the $dsDNA_2$/GQD/$dsDNA_1$/Au electrode, we investigated the effect of the scan rate. Figure 4a shows cyclic voltammograms of DA in 0.1 M phosphate buffer (pH 7.4) at the $dsDNA_2$/GQD/$dsDNA_1$/Au electrode with different scan rates. The anodic and cathodic peak currents increase with increasing scan rate. The corresponding plots of the peak currents against scan rate are shown in Fig. 4b. Both the anodic

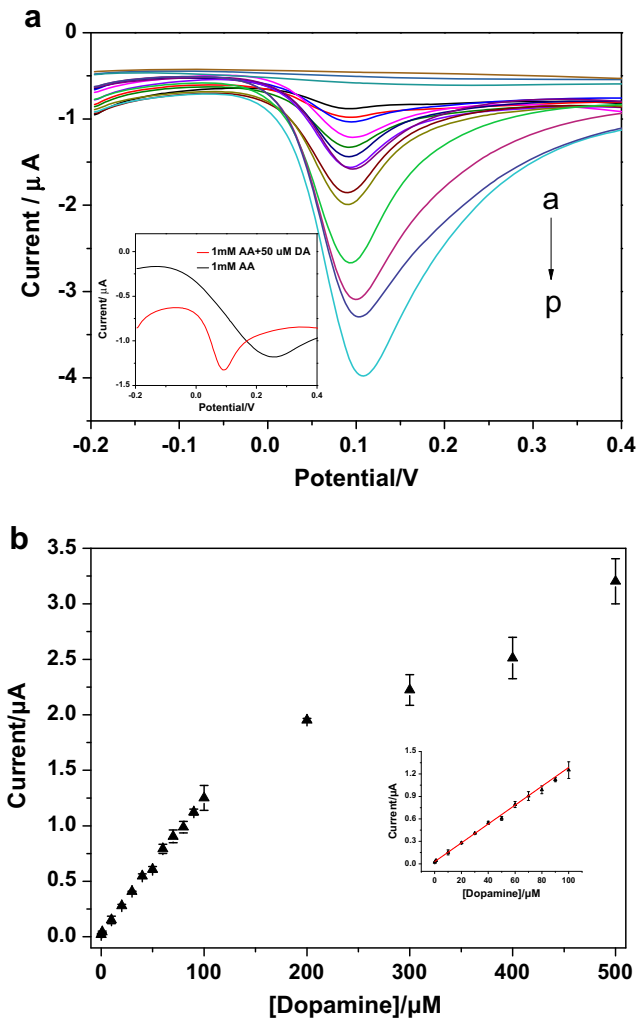

Fig. 5 **a** Differential Pulse Voltammetry at the $dsDNA_2$/GQD/$dsDNA_1$/Au electrode of AA (1 mM) and DA with increasing concentrations (from (a) to (l): 0.1, 1, 10, 20, 30, 40, 50, 60, 70, 80, 90, 100, and then with 100 μM increments until 500 μM). Inset: Differential Pulse Voltammetry at the $dsDNA_2$/GQD/$dsDNA_1$/Au electrode for AA (1 mM) in the presence of DA with different concentrations (0 μM and 10 μM). **b** Dependence of the response currents of the $dsDNA_2$/GQD/$dsDNA_1$/Au electrode on the concentration of DA (from 0.1 μM to 500 μM). Inset: linear relationship between peak current and concentration (from 0.1 μM to 100 μM)

Table 3 Comparison with other sensors for DA detection

	Linear range (μM)	Detection limit (nM)	References
Gr–PPy-Fe_3O_4 /GCE	0.007–2.0	2.33	[35]
G-CN/GCE	0.1–100	50	[36]
MnO_2-GO/GCE	0.5–2500	170	[37]
Polymer-CN/GCE	5–1000	2300	[38]
Porous gold nanosheet/GCE	2.0–298	280	[39]
AuNPs/carton nano/GCE	0.03–6.0	10	[40]
naphthoquinone/Au	1–100	40	[41]
rGO /GCE	0.05–50	10	[42]
PPy-RGO/GCE	0.01–10	1	[43]
HAu-G/GCE	0.08–600	50	[44]
ERGO/GCE	0.5–60	500	[45]
RGO/Pd-NPs/GCE	0–150	230	[46]
DNA/GQDs/DNA/Au	0.1–100	30	This work

and cathodic peak currents follow a linear relationship with scan rate in a range 0.005–1 V s^{-1} and with linear correlation coefficients of 0.9993 and 0.9986, respectively. This indicates that the electrochemical oxidation of DA at the $dsDNA_2$/GQD/$dsDNA_1$/Au electrode is a surface-controlled process rather than a diffusion-controlled process [30].

Electrochemical determination of DA

A major problem in electrochemical detection of DA is interference from ascorbic acid (AA), because the two molecules oxidize at very similar potentials, resulting in overlapping voltammetric responses. The DPV responses of different concentrations of DA with AA at the $dsDNA_2$/GQD/$dsDNA_1$/Au electrode are shown in Fig. 5(a). Only the peak corresponding to the oxidation of DA can be seen. Therefore, interference from AA can be completely eliminated by using the bio-nanostructure layer. The lack of AA oxidation is due to two factors: (1) negatively charged DNA and COO^- groups on the GQDs electrostatically repel negatively charged AA (pKa = 4.2) and inhibit interfacial charge transfer; and (2) it is difficult for AA to approach the sensing interface by π-interaction because AA does not contain an aromatic ring.

Electrochemical oxidation of DA occurs at ca. 0.10 V and the peak current of DA is proportional to the concentration of DA (c_{DA}) in the range 0.1–100 μM, which can be described by the linear equation I_{pa} (μA) = 0.01258c_{DA} + 0.02891 (μA) with a correlation coefficient of 0.9992, as shown in Fig. 5(b). The limit of detection (LOD) is calculated to be 30 nM based on the signal-to-noise ratio of 3. Compared with other DA sensors (Table 3), the DNA-GQD self-assembled electrochemical sensor in this work is more sensitive, and has a relatively low LOD and concentration range of DA. Moreover, compared with previously reported DA sensors [32–34], the sensor presented in this work has the following merits: (1) The gold surface serving as the basis for the development of a high throughput detection chip is more convenient, and (2) chemical bonding means that the sensor has better stability and reproducibility than sensors fabricated by physical adsorption of graphene-related materials.

The sensor has good reproducibility, with a relative standard deviation (RSD) of 3.8% for eight different electrodes. The stability of the sensor was also tested (shown in Fig. S6). The peak current remained 97% following storage of the $dsDNA_2$/GQD/$dsDNA_1$/Au electrode at 4 °C for 21 days. The use of the method in the analysis of real samples was also investigated by the direct analysis of DA in human serum samples. All the serum samples were diluted 100 times with 0.1 M phosphate buffer (pH 7.4) before measurement. The experimental results (obtained from the average value of three independent tests) are described in Table 4. The recoveries presented acceptable values from 92.8% to 107.04%, with relative

Table 4 Determination of DA in human serum samples (n = 3)

Serum sample	DA in diluted sample (μM)	Added (μM)	Found (μM)	R.S.D. (%)	Recovery (%)
1	0	10	9.28	5.3	92.8
2	0	25	26.76	1.5	107.04
3	0	50	48.42	2.3	96.84

standard deviations of 1.45–5.28% (n = 3), indicating that the assay can potentially be used for determination of DA in real samples under the experimental conditions described.

Conclusion

A 3D structure of graphene and DNA immobilized on a gold electrode and fabricated by layer-by-layer superposition is reported. AFM and electrochemical analysis clearly show that graphene-DNA possesses an ordered 3D bio-nano-structure and high charge-transfer performance. Moreover, the $dsDNA_2$/GQD/$dsDNA_1$/Au electrode was successfully used to determine DA in the presence of a high concentration of AA. It showed excellent electrocatalytic activity for determining DA and a response to the interfering agent AA was entirely absent. The electrochemical response to DA shows a good linear range and a very low detection limit. We believe that this bio-nano-structure and the electrochemical information provided here can serve as a benchmark for graphene-DNA sensor performance.

Acknowledgments This work was financially supported by the National Natural Science Foundation of China (No. 21475006, 21375005, 21527808).

Compliance with ethical standards The author(s) declare that they have no competing interests.

References

1. Xu T, Zhang Q, Zheng J, Lv Z, Wei J, Wang A, Feng J (2014) Simultaneous determination of dopamine and uric acid in the presence of ascorbic acid using Pt nanoparticles supported on reduced graphene oxide. Electrochim Acta 115:109–115
2. Sanghavi B, Wolfbeis O, Hirsch T, Swami N (2015) Nanomaterial-based electrochemical sensing of neurological drugs and neurotransmitters. Microchim Acta 182:1–41
3. Geim, A.K., Novoselov, K.S (2007) The rise of graphene. Nat Mater 6(3):183–191
4. Khomyakov PA, Giovannetti G, Rusu PC, Brocks GV, Van den Brink J, Kelly PJ (2009)) First-principles study of the interaction and charge transfer between graphene and metals. Phys Rev B 79(19):195425
5. Slinker, J. D., Muren, N.B., Renfrew E. S.; Barton, J. K (2011) DNA charge transport over 34 nm. Nat Chem 3:228–233
6. Premkumar, T., Geckeler, K.E (2012) Graphene–DNA hybrid materials: assembly, applications, and prospects. Prog Polym Sci 37(4):515–529
7. Lee, S.H., Kim, H.W., Hwang, J.O., Lee, W.J., Kwon, J., Bielawski, C.W., Ruoff, R.S., Kim, S.O (2010) Three-dimensional self-assembly of graphene oxide platelets into mechanically flexible Macroporous carbon films. Angew Chem 122(52): 10282–10286
8. Xu Y, Wu Q, Sun Y, Bai H, Shi G (2010) Three-dimensional self-assembly of graphene oxide and DNA into multifunctional hydrogels. ACS Nano 4(12):7358–7362
9. Sun X, Liu Z, Welsher K, Robinson JT, Goodwin A, Zaric S, Dai H (2008) Nano-graphene oxide for cellular imaging and drug delivery. Nano Res 1(3):203–212
10. Liu X, Aizen R, Freeman R, Yehezkeli O, Willner I (2012) Multiplexed aptasensors and amplified DNA sensors using functionalized graphene oxide: application for logic gate operations. ACS Nano 6(4):3553–3563
11. He Q, Wu S, Yin Z, Zhang H (2012) Graphene-based electronic sensors. Chem Sci 3(6):1764–1772
12. Patil AJ, Vickery JL, Scott TB, Mann S (2009) Aqueous stabilization and self-assembly of graphene sheets into layered bionanocomposites using DNA. Adv Mater 21(31):3159–3164
13. Subramanian P, Lesniewski A, Kaminska I, Vlandas A, Vasilescu A, Niedziolka-Jonsson J, Pichonat E, Happy H, Boukherroub R, Szunerits S (2013) Lysozyme detection on aptamer functionalized graphene-coated SPR interfaces. Biosens Bioelectron 50:239–243
14. Sarma SD, Adam S, Hwang EH, Rossi E (2011) Electronic transport in two-dimensional graphene. Rev Mod Phys 83(2):407
15. Chen D, Tang L, Li J (2010) Graphene-based materials in electrochemistry. Chem Soc Rev 39(8):3157–3180
16. Kim Y, Bong S, Kang Y, Yang Y, Mahajan RK, Kim JS, Kim H (2010) Electrochemical detection of dopamine in the presence of ascorbic acid using graphene modified electrodes. Biosens Bioelectron 25(10):2366–2369
17. Sheng Z, Zheng X, Xu J, Bao W, Wang F, Xia X (2012) Electrochemical sensor based on nitrogen doped graphene: simultaneous determination of ascorbic acid, dopamine and uric acid. Biosens Bioelectron 34(1):125–131
18. Wang Y, Li Y, Tang L, Lu J, Li J (2009) Application of graphene-modified electrode for selective detection of dopamine. Electrochem Commun 11(4):889–892
19. Wu L, Feng L, Ren J, Qu X (2012) Electrochemical detection of dopamine using porphyrin-functionalized graphene. Biosens Bioelectron 34(1):57–62
20. Caballero-Diaz, E., Benitez-Martinez, S., Valcarcel, M., Rapid and simple nanosensor by combination of graphene quantum dots and enzymatic inhibition mechanisms, Sens Actuators B Chem, 2017, 240, 90–99
21. Lin XQ, Lu LP, Jiang XH (2003) Voltammetric behavior of dopamine at ct-DNA modified carbon fiber microelectrode. Microchim Acta 143:229–235
22. Lu LP, Wang SQ, Lin XQ (2004) Fabrication of layer-by-layer deposited multilayer films containing DNA and gold nanoparticle for norepinephrine biosensor. Anal Chim Acta 519:161–166
23. Furst, A.L., Hill, M.G., Barton, J.K (2013) DNA-modified electrodes fabricated using copper-free click chemistry for enhanced protein detection. Langmuir 29(52): 16141–16149
24. Lu LP, Xu LH, Kang TF, Cheng SY (2012) Investigation of DNA damage treated with perfluorooctane sulfonate (PFOS) on ZrO2/DDAB active nano-order film. Biosens Biolectron 35:180–185
25. Xie R, Wang Z, Zhou W, Liu Y, Fan L, Li Y, Li X (2016) Graphene quantum dots as smart probes for biosensing. Anal Methods 8: 4001–4016
26. Laviron E (1979) General expression of the linear potential sweep voltammogram in the case of diffusionless electrochemical systems. J Electroanal Chem Interfacial Electrochem 101(1):19–28
27. Song Y, Wan L, Wang Y, Zhao S, Hou H, Wang L (2012) Electron transfer and electrocatalytics of cytochrome c and horseradish peroxidase on DNA modified electrode. Bioelectrochemistry 85:29–35
28. sPheeney, C.G., Barton, J.K (2013) Intraduplex DNA-mediated electrochemistry of covalently tethered redox-active reporters. J Am Chem Soc 135(40): 14944–14947
29. Pattnaik S, Swain K, Lin ZQ (2016) Graphene and graphene-based nanocomposites: biomedical applications and biosafety. J Mater Chem B 4:7813–7831

30. Liu S, Yan J, He G, Zhong D, Chen J, Shi L, Zhou X, Jiang H (2012) Layer-by-layer assembled multilayer films of reduced graphene oxide/gold nanoparticles for the electrochemical detection of dopamine. J Electroanal Chem 672:40–44
31. Wang H, Ren F, Yue R, Wang C, Zhai C, Du Y (2014) Macroporous flower-like graphene-nanosheet clusters used for electrochemical determination of dopamine. Colloids Surf A Physicochem Eng Asp 448:181–185
32. Feng X, Zhang Y, Zhou J, Li Y, Chen S, Zhang L, Ma Y, Wang L, Yan X (2015) Three-dimensional nitrogen-doped graphene as an ultrasensitive electrochemical sensor for the detection of dopamine. Nanoscale 7(6):2427–2432
33. Han HS, Ahmed MS, Jeong H, Jeon S (2015) The determination of dopamine in presence of serotonin on dopamine-functionalized electrochemically prepared graphene biosensor. J Electrochem Soc 162(4):B75–B82
34. Sun J, Li L, Zhang X, Liu D, Lv S, Zhu D, Wu T, You T (2015) Simultaneous determination of ascorbic acid, dopamine and uric acid at a nitrogen-doped carbon nanofiber modified electrode. RSC Adv 5(16):11925–11932
35. Wang Y, Zhang Y, Hou C, Liu M (2016) Ultrasensitive electrochemical sensing of dopamine using reduced graphene oxide sheets decorated with p-toluenesulfonate-doped polypyrrole/Fe3O4 nanospheres. Microchim Acta 183(3):1145–1152
36. Mani V, Govindasamy M, Chen SM, Karthik R, Huang ST (2016) Determination of dopamine using a glassy carbon electrode modified with a graphene and carbon nanotube hybrid decorated with molybdenum disulfide flowers. Microchim Acta 183:2267–2275
37. Rao D, Zhang X, Sheng Q, Zheng J (2016) Highly improved sensing of dopamine by using glassy carbon electrode modified with MnO2, graphene oxide, carbon nanotubes and gold nanoparticles. Microchim Acta 183(9):2597–2604
38. Liu R, Zeng X, Liu J, Luo J, Zheng Y, Liu X (2016) A glassy carbon electrode modified with an amphiphilic, electroactive and photosensitive polymer and with multi-walled carbon nanotubes for simultaneous determination of dopamine and paracetamol. Microchim Acta 183:1543–1551
39. Zhang ZL, Feng JX, Wang AJ, Wei J, Lv ZY, Feng JJ (2015) A glassy carbon electrode modified with porous gold nanosheets for simultaneous determination of dopamine and acetaminophen. Microchim Acta 182:589–595
40. Xu Y, Hun X, Liu F, Wen X, Luo X (2015) Aptamer biosensor for dopamine based on a gold electrode modified with carbon nanoparticles and thionine labeled gold nanoparticles as probe. Microchim Acta 182:1797–1802
41. Hammami A, Sahli R, Raouafi N (2016) Indirect amperometric sensing of dopamine using a redox-switchable naphthoquinone-terminated self-assembled monolayer on gold electrode. Microchim Acta 183:1137–1144
42. Kumar MK, Prataap RV, Mohan S, Jha SK (2016) Preparation of electro-reduced graphene oxide supported walnut shape nickel nanostructures, and their application to selective detection of dopamine. Microchim Acta 183(5):1759–1768
43. Qian T, Wu SS, Shen J (2013) Facilely prepared polypyrrole-reduced graphite oxide core-shell microspheres with high dispersibility for electrochemical detection of dopamine. Chem Commun 49:4610–4612
44. Zhu WC, Chen T, Ma XM, Ma HY, Chen SH (2013) Highly sensitive and selective detection of dopamine based on hollow gold nanoparticles-graphene nanocomposite modified electrode. Colloids Surf B: Biointerfaces 111:321–326
45. Yang L, Liu D, Huang J et al (2014) Simultaneous determination of dopamine, ascorbic acid and uric acid at electrochemically reduced graphene oxide modified electrode. Sensors Actuators B Chem 193:166–172
46. Palanisamy S, Ku S, Chen SM (2013) Dopamine sensor based on a glassy carbon electrode modified with a reduced graphene oxide and palladium nanoparticles composite. Microchim Acta 180: 1037–1042